Colloid Polym Sci (2008) 286:1079–1092
DOI 10.1007/s00396-008-1871-5

ORIGINAL CONTRIBUTION

The collapse transition of poly(styrene-*b*-(*N*-isopropyl acrylamide)) diblock copolymers in aqueous solution and in thin films

K. Troll · A. Kulkarni · W. Wang · C. Darko · A. M. Bivigou Koumba · A. Laschewsky · P. Müller-Buschbaum · C. M. Papadakis

Received: 14 December 2007 / Revised: 13 March 2008 / Accepted: 14 March 2008 / Published online: 30 May 2008

Abstract The thermal behavior of a poly(styrene-*b*-*N*-isopropyl acrylamide) diblock copolymer was studied in aqueous solution as well as in thick and in thin films. The polymer was synthesized using reversible addition–fragmentation chain transfer. The critical micelle concentration in aqueous solution was determined using fluorescence correlation spectroscopy. The lower critical solution temperature (LCST) of micellar solutions was detected using microcalorimetry and turbidimetry at 31 °C. Using dynamic light scattering, the collapse of the micelles at the LCST as well as their clustering above was observed. These findings were corroborated with small-angle X-ray scattering. In thick films immersed in water, similar findings were made. In a thin film, however, the LCST is depressed and is found at 26–27 °C.

Keywords Block copolymers · Responsive polymers · Scattering

K. Troll · A. Kulkarni · W. Wang · C. Darko · P. Müller-Buschbaum · C. M. Papadakis (✉)
Physikdepartment E13, Technische Universität München, James-Franck-Str. 1,
Garching 85747, Germany
e-mail: Christine.Papadakis@ph.tum.de

A. M. Bivigou Koumba · A. Laschewsky
Institut für Chemie, Universität Potsdam,
Karl-Liebknecht-Str. 24-25,
Golm/Potsdam 14476, Germany

Introduction

The collapse transition of polymers with lower critical solution temperature (LCST) behavior is of great interest for a number of purposes where a strong change of volume is desired even for small changes of temperature, such as valves in microfluidics, but also for the release of drugs in the body or as sensors. A polymer that is a promising candidate in this context is poly(*N*-ispropylacrylamide), PNIPAM [1]. It exhibits an LCST of about 32 °C that is attributed to alterations in the hydrogen-bonding interactions of the amide group [1–4]. In cross-linked hydrogels, its LCST temperature in water was found to be 33.2 °C upon heating [5]. Significant macroscopic volume changes have been obtained and have been characterized by calorimetry, dynamic light scattering, and small-angle neutron scattering [6–9]. Upon the collapse, water is released from the gel. In thin-film geometry, such gels are of interest for applications such as thermosensitive surfaces, artificial pump and muscles, light modulation systems, and optical switches.

Because the response times of such thermosensitive hydrogels depend strongly on the size of the gel [10], for some bulk applications, they are too long. A recent trend in creating responsive, polymeric hydrogels is thus to decrease the size of the responsive units. In bulk systems, this has been achieved by synthesizing microgels [11], colloidal particles with a cross-linked hydrophobic core and a cross-linked hydrophilic and responsive shell [12–15] or by exploiting the potential for self-assembly of amphiphilic block copolymers containing the responsive PNIPAM block. In thin films, the volume is already decreased by the very limited film thickness.

Block copolymer systems offer additional possibilities due to their potential to self-assemble to core-shell micelles. It is interesting to study their interaction with solid interfaces breaking translational symmetry. It is advantageous to use PNIPAM together with a hydrophobic block [16–19]. In most cases, polystyrene (PS) was chosen as the hydrophobic block, and diblock copolymers P(S-*b*-NIPAM) [16, 18, 20] and, occasionally, also triblock copolymers P(S-*b*-NIPAM-*b*-PS) were studied [19, 20]. In the present work, we combine structural studies of a P(S-*b*-NIPAM) diblock copolymer in solution, in a thick film, and in thin-film geometry.

The aggregation behavior of P(S-*b*-NIPAM) diblock copolymers in dilute aqueous solution depends strongly on the weight fraction of the PNIPAM block: Whereas a diblock copolymer with a PNIPAM weight fraction of 63% forms crew-cut core-shell micelles [16], a diblock copolymer with a weight fraction of 88% forms seemingly unstructured, large aggregates [16]. In contrast, a P(S-*b*-NIPAM) diblock copolymer with a weight fraction of 65% but higher block molar masses than the one cited above was reported to form core-shell micelles [18]. Details of the preparation conditions (dialysis from organic solvent or dissolution in organic solvent and subsequent mixing with water) may have an influence on the resulting structure, and it seems that the aggregate formation is a delicate process. Another diblock copolymer was created by hydrolysis of a trithiocarbonate group located in the center of the PNIPAM block of a P(S-*b*-NIPAM-*b*-PS) triblock copolymer [20]. The authors compared the collapse transition of the micelles formed by triblock and then the diblock copolymers. However, one may suspect that, as the hydrolysis was performed in the micellar solution formed by the triblock copolymers, there is a risk that, after hydrolysis, the diblock copolymer micelles are not in equilibrium.

We present in this paper a study of the self-assembly and the thermal behavior of a P(S-*b*-PNIPAM) diblock copolymer that was synthesized using reversible addition–fragmentation chain transfer (RAFT). The molar masses of the PS and the PNIPAM block are 5,000 and 18,000 g/mol; the weight fraction of PNIPAM is thus 78%. We compare the thermal behavior in fully hydrated state, i.e., in aqueous solution, with the one in a thick film, both dry and immersed in water, and a thin film in saturated water vapor. In solution, we have determined the critical micelle concentration (CMC) by fluorescence correlation spectroscopy, the collapse transition of the PNIPAM block using microcalorimetry and turbidimetry, as well as the micellar size in dependence of temperature using dynamic light scattering and small-angle X-ray scattering (SAXS). The temperature-dependent structures in dry and wet thick films were investigated using SAXS and the thermal behavior of a thin film in the vapor-swollen state using atomic force microscopy (AFM) and optical interference measurements.

Experimental section

Materials

Carbon disulfide (75–15–0; 99.9%, Acros Organics), 1-bromopropane (106–94–5; 99%, Sigma-Aldrich), 4-methoxy-α-toluenethiol (6258–60–2; Sigma-Aldrich), dichloromethane (75–09–2; Acros Organics), triethylamine (121–44–8; 99%, Acros Organics), and magnesium sulfate (7487–88–9; 97%, Acros Organics) were used as received. Tetrahydrofurane (THF) was distilled over K–Na. Styrene (100–42–5; 99%, Sigma-Aldrich) was purified by passing through a column filled with basic Al_2O_3 (1344–28–1; activated, 50–200 micron, Acros Organics). *N*-Isopropylacrylamide (2210–25–5; NIPAM, 99%, Acros Organics) was recrystallized from hexane and dried in vacuo. AIBN (Wako) was recrystallized from methanol and dried in vacuo.

Synthesis of RAFT agent CTA1

In analogy to a general procedure [21, 22], triethylamine (6.4 ml, 0.068 mol) was dropped to a stirred mixture of 4-methoxy-α-toluenethiol (10.0 g, 0.064 mol), CS_2 (4 ml, 0.066 mol), and dry CH_2Cl_2 (20 ml) at room temperature. The solution became yellow/orange as the addition proceeded with formation of the intermediate triethylammonium trithiocarbonate. After 30 min of stirring, 1-bromopropane (8.0 g, 0.064 mol) was added slowly, causing the mixture to thicken with formation of the bromide salt. The reaction mixture was stirred for another 16 h then diluted with additional CH_2Cl_2 (20 ml) before washing sequentially with three portions of 100 ml of deionized water. The solution was dried over $MgSO_4$, concentrated by evaporation, and passed over a short column filled with basic alumina. The solvent was removed by rotary evaporation to give an orange oil.

Yield, 15.68 g (90%); elemental analysis ($C_{12}H_{16}OS_3$, M_r=272.46), calculated C=52.90%; H=5.92%, S=35.31%; found, C=53.13%, H=5.90%, and S=34.63%; MS (EI, negative ions), m/z=272.45; ^{1}H-NMR (300 MHz in $CDCl_3$, δ in ppm), δ=1.12 (t, 3H, CH_3–), 1.83 (m, 2H S–C–CH_2–), 3.45 (t, 4H, S–CH_2–), 3.88 (s, 3H, CH_3O–), 4.66 (s, 2H, CH_2–aryl), 6.93 (d, 2H, −CH=C–O–), 7.34 (d, 2H,=CH–C=C–O–); ^{13}C-NMR (75 MHz in $CDCl_3$, δ in ppm), δ=13.41 (CH_3–), 21.50 (CH_3–CH_2–), 38.72 (–S–CH_2–alkyl), 40.92 (–S–CH_2–aryl), 114.05 (–CH=C–O aryl), 126.60 (=C< aryl), 130.38 (=CH–C=C–O aryl), 159.12 (=C–O aryl), 223.90 (–S–(−(C=S)–S–); UV–vis (in CH_2Cl_2), bands at λ_{max1}=310 nm ($\pi-\pi^*$, ε=16,100 l mol^{-1} cm^{-1}), λ_{max2}=433 nm ($n-\pi^*$, ε=62.5 l mol^{-1} cm^{-1}).

Synthesis of poly(styrene) macroRAFT agent

Styrene (10.01 g; 0.096 mol) and RAFT agent (0.23 g; 8.33×10^{-4} mol) were accurately weighed and then transferred to a 100-ml one-necked round-bottom flask equipped with a magnetic stirrer. The homogeneous mixture was sealed with a rubber septum, and the contents were degassed with argon for 25 min to eliminate oxygen. The flask was then immersed in an oil bath hold at 110 °C. After 18 h, the polymerization was quenched by placing the flask into liquid nitrogen. The reaction mixture was diluted with acetone and precipitated in methanol. The precipitation was repeated twice, and the polymer was finally dried in vacuo at 50 °C for 16 h. Yield 4.5 g (45.3%).

Polymer chain extension with NIPAM

In a typical polymerization, NIPAM (10.05 g; 8.83×10^{-2} mol), macroRAFT agent (2.48 g; 5×10^{-4} mol) and AIBN (0.0082 g; 5×10^{-5} mol) were dissolved in THF (53 ml). The mixture was deoxygenated by bubbling with argon for 55 min and immersed into an oil bath preheated to 65 °C. After 37 h, the reaction was quenched by placing the flask into liquid nitrogen. The reaction mixture was diluted with acetone and precipitated in diethyl ether (500 ml). The polymer was collected by suction filtration, dissolved in acetone and dialyzed for 3 days, and freeze-dried to give a white-off powder.

Yield, 8.57 g (86%); elemental analysis: found, C= 66.85%, H=9.32%, N=9.30%, S=0.38% [from C/N ratio, molar ratio Styrene (C_8H_8, M_r=104.15)/NIPAM ($C_6H_{11}NO$, M_r=113.16)=1/3.35].

Materials and methods

Spectroscopy

^1H and ^{13}C NMR spectra were taken with an apparatus Bruker Avance 300 (300 MHz). Mass spectra were recorded by a GC/MS-system Trace DSQII (Thermo Scientific). UV–vis spectra were recorded on a spectrophotometer Cary-1 (Varian) equipped with temperature controller (Julabo F-10). Quartz cuvettes (Suprasil, Hellma, Germany) with an optical path length of 10 mm were used.

Size-exclusion chromatography

Size-exclusion chromatography (SEC) of the polymers was run in *N*,*N*-dimethylacetamide containing 0.1% LiBr as eluent at a column temperature of 45 °C, with a setup consisting of an Agilent 1200 isocratic pump, an Agilent 1200 refractive index detector, and two GRAM columns (10 μm, 8×300 mm, pore sizes 100 and 1,000, PSS GmbH, Mainz, Germany). The SEC setup was calibrated using low polydispersity polystyrene standards (PSS GmbH). Assuming an ideal RAFT mechanism [23] and that (a) the amount of initiator-derived polymer chains is negligible and (b) the obtained yields correspond to monomer conversion, the theoretically expected number average molar mass M_n^{theor} can be calculated in very good approximation as

$$M_{theor} = \frac{\text{conversion} \times M_{monomer} \times [M]}{\text{CTA}} + M_{CTA} \quad (1)$$

where $[M]$ is the initial concentration of the monomer, [CTA] is the concentration of RAFT agent, $M_{Monomer}$ is the molar mass of the monomer, and M_{CTA} is the molar mass of the chain transfer agent.

Microcalorimetry

Microcalorimetry experiments were performed using a VP-DSC instrument from Microcal, LLC, USA. An amount of ~0.517 ml of polymer solution was placed into the sample cell. The scan rate was varied between 0.5 and 1.0 K/min. Both heating and cooling scans were performed between 15 and 48 °C. The measured baseline from water was subtracted.

Turbidimetry

Turbidity measurements were performed on a temperature-controlled turbidimeter (model TP1, E. Tepper, Germany) with heating and cooling rates of 1.0 K/min, respectively. The transmittance of polymer solutions was set automatically to 100% at the beginning of each measurement. Temperatures are precise within 0.5 K.

Fluorescence correlation spectroscopy

For fluorescence correlation spectroscopy (FCS), a ConfoCor 2 from Carl Zeiss Jena GmbH was used together with an Ar^+ laser (λ=488 nm), a pinhole with a diameter of 70 μm, a BP 530–600 emission filter, and an HFT 488 plate beam splitter. The autocorrelation functions of the fluctuations of the fluorescence intensity, $G(\tau)$, were analyzed by fitting the following expression [24]:

$$G(\tau) = 1 + \frac{1}{N} \times \left[1 + \frac{T_T}{1 - T_T} \exp\left(-\frac{\tau}{\tau_T}\right)\right] \times \sum_{i=1}^{n} \frac{\rho_i}{\left(1 + \frac{\tau}{\tau_{D,i}}\right)\sqrt{1 + \frac{\tau}{(z_0/w_0)^2 \tau_{D,i}}}} \quad (2)$$

where N is the total number of fluorescent particles in the observation volume, n the number of different fluorescent

species, $\tau_{D,i}$ the diffusion time of the ith species, ρ_i the amplitude of the ith species, and z_0 and w_0 the half-height and half-width of the observation volume, respectively. T_T and τ_T are the triplet fraction and time, respectively. From the fit, the values were found to be in the range T_T= 0.1–0.2 and τ_T=1–3 μs. w_0 was determined before each session by measuring the diffusion time of Rhodamine 6G (Sigma-Aldrich, $D_{Rh6G}=2.8\times10^{-10}$ m^2 s^{-1} [25]), $\tau_{D,Rh6G}$, and by using $w_0 = \left(4D_{Rh6G} \times \tau_{D,Rh6G}\right)^{1/2}$. A value $w_0 \cong 0.2$ μm was obtained. The ratio z_0/w_0 determined from the fit to the Rhodamine 6G correlation function in water was typically 5–6. A stock solution of Rh6G (1 μM) was prepared in deionized and filtered water. It was mixed with a previously prepared aqueous polymer solution such that the concentration of Rh6G was 50 nM, and the one of the polymer was varied between 0.1 and 8 μM. Measurements were carried out at room temperature.

Dynamic light scattering

For dynamic light scattering (DLS) experiments, the polymer solutions were filtered into previously de-dusted scattering cells. Temperature-resolved experiments were performed in polarized geometry using an ALV-5000/E correlator together with a goniometer with an index-matching vat filled with toluene. The light source was a Nd:YAG laser operated at λ=532 nm. The scattered light was detected at a scattering angle θ=90° using photomultipliers operated in pseudo-cross-correlation mode to which the signal was fed by optical fibers with a beam splitter. At each temperature, ten measurements of 0.5 min duration were performed. After each temperature change, the waiting time was 20 min. The correlation functions were analyzed by numerical inverse Laplace transformation using the REPES program included in the GENDIST software package [26, 27]. From the measured intensity autocorrelation function, $G_2(t)$, it calculates the distribution of hydrodynamic radii, $A(R_H)$, using the Stokes–Einstein relation:

$$r_H = \frac{k_B T}{6\pi\eta} \times \tau q^2 \tag{3}$$

where k_B is Boltzmann's constant, T the absolute temperature, η the temperature-dependent viscosity of water, and τ the relaxation time of the decay in the correlation curve. q is the modulus of the scattering vector given by $q = 4\pi n \times \sin(\theta/2)/\lambda$, with n the measured refractive index of the sample. Unless otherwise stated, the probability to reject was chosen at 0.5; i.e., the most probable solution was chosen. From the centers of gravity of the peaks in $A(R_H)$, the average R_H value is obtained.

Small-angle X-ray scattering

SAXS experiments were performed at beam line A2, HASYLAB at DESY in Hamburg, Germany. An X-ray beam with a wavelength of λ=1.5 Å and a size of 2.0× 0.8 mm was used. A linear, position-sensitive gas detector was mounted in 3.00-m distance from the sample. As a beamstop, a piece of lead was used. With the setup described, the accessible q range was 0.13–1.3 nm^{-1}. The background was determined using the water used for the solutions or the dialysis. The q calibration was performed using dry collagen. Aqueous polymer solutions were mounted between two pieces of kapton foil resulting in a sample thickness of 1 mm. Measurements were carried out between 20 and 40 °C. Each measurement took 10 min with waiting times of 10 min in-between.

The radius of gyration of the micelles at low temperatures was determined using the Guinier approximation [28] in a range of 0.13–0.20 nm^{-1}. For the analysis of the entire SAXS curves, the software Scatter 2.0 was used [29]. The electron densities are 337, 354, and 333 electrons/nm^3 for PS, PNIPAM, and H_2O, respectively. The curve of a micellar solution in the swollen state at 20 °C was fitted by modeling the micellar core as spherical with a homogeneous electron density, whereas the electron density in the shell has an algebraic decay $\rho \propto r^{\alpha}$ where r is the radial coordinate and α is negative [29]. For the collapsed state at 40 °C, a model for a homogeneous spherical micelle was used, and the interaction between micelles was described using a Percus–Yevick structure factor.

Thick films were deposited on kapton foil, which was pre-cleaned by water, ethanol, and dioxane by solution casting from dioxane (polymer concentration, 109.6 mg/ml). The dry film thickness was 0.1–0.5 mm. The films were mounted in the same, nearly closed kapton cell as the solutions and were studied in transmission. To investigate the swollen state, water was added to the cell, such that the film was immersed in water. Measurements were carried out between 20 and 40 °C. Each measurement took 10 min with 50 min waiting time.

Transmission electron microscopy

Transmission electron microscopy (TEM) was carried out using a JEOL JEM2011 operated at 120 kV. Samples were prepared by placing a droplet (5 μl) of a 0.1-mg/ml aqueous solution of P(S-*b*-NIPAM) on a hole carbon film (Quantifoil, Jena Germany) supported by a copper grid. The excess solution was blotted with a piece of filter paper. The resulting thin (approximately 50 nm) liquid film in the holes of the carbon film was then air-dried at room temperature.

Optical interference measurements

The film thickness and the optical constants, n and k, were measured with a Filmetrics F20 thin-film measurement system (Filmetrics Inc., San Diego, CA, USA). The spot size of the light beam was adjustable from 500 μm to 1 cm. The characteristic intensity oscillations in the refractance spectrum were analyzed in a wavelength regime from 340 to 1,100 nm.

Thin P(S-*b*-NIPAM) films were prepared on Si(100) substrates (n-type, Silchem) with a thin oxide layer on top. The substrates were cleaned with a basic protocol [30] before coating them by spin-coating out of 1,4-dioxane (2,000 rpm, 30 s). Smooth and continuous films resulted. These films were mounted in a temperature-controlled swelling chamber with a water reservoir inside, i.e., in saturated water vapor atmosphere. The thicknesses of the dry film and of the swollen film were determined as a function of temperature. Starting at room temperature, the sample was allowed to equilibrate after each temperature increase by ΔT=1 °C for 30 min. Equilibration was concluded from the absence of any changes in the spectra of the optical interference measurements. The resulting spectra were fitted including changes in the refractive index due to incorporation of water. The optical constants of P(S-*b*-NIPAM) were taken as reference for the dry film.

Results and discussion

Synthesis and molecular characterization

The preparation of the amphiphilic block copolymer by the RAFT method using the new monofunctional trithiocarbonate CTA1 is sketched in Scheme 1. In the first step, styrene is thermally polymerized in the presence of the appropriate amount of CTA1, which may be described by the general formula R–S–C(=S)–Z and which, in this, notation bears the *p*-methoxybenzyl residue as reinitiating group R and the inert *n*-propylthio moiety as activating Z group. After isolation and purification, the formed polystyrene is engaged as macroRAFT agent macroCTA1 in the subsequent polymerization of NIPAM initiated by AIBN to produce the block copolymer P(S-*b*-NIPAM).

The progress of the polymerization can be followed by SEC and ^{1}H-NMR (Figs. 1, 2, and 3). The judicious choice of the R and Z substituents of the RAFT agent allows to see their incorporation in the formed polymers. After the first step, the ^{1}H-NMR spectrum of the polystyrene macroCTA1 clearly shows characteristic signals at approximately 3.8 ppm, indicative of the methoxy moiety of the initiating R group, whereas the signals at approximately 3.4 and 0.95 ppm are indicative of the –S–CH_2– and the terminal CH_3– groups, respectively, of the *n*-propylthio Z fragment (cf. Figs. 1 and 2). Integration of these signals in comparison, e.g., to the aromatic protons of the polystyrene (h–k) enables to calculate the molar mass via end-group analysis. In the case of the Z group, the signal of the –S–CH_2– moiety is preferred for quantification over the one of the CH_3 moiety, as the latter is not fully resolved from the intense polymer signals between 1.0 and 2.8 ppm. Accordingly, a number average molar mass M_n of 5,850 is calculated considering the signal of the R group, and a value of 6,200 is calculated for M_n, considering the signal of the Z group. The analysis by SEC shows a monomodal, relatively narrow molar mass distribution, with an M_n value of 5,000 and a polydispersity index PDI of 1.2. Assuming an ideal RAFT mechanism, the theoretically expected number average molar mass M_n^{theor} is calculated as 5,400; this value is a lower estimate, as any polymer loss during isolation and purification will reduce the yield and thus the apparent conversion. The good agreement between all these values within experimental precision demonstrates not only the good control over the molar mass but also the high extent of end-group functionalization of macroCTA1, as needed for the synthesis of the block copolymers.

Successful chain extension of the macroRAFT1 agent by NIPAM is revealed by SEC. The trace of the elugram of the block copolymer is significantly shifted in comparison to the trace of macroRAFT1. It shows a monomodal molar mass distribution with a PDI value of 1.47 and gives an apparent value of $M_n^{app} = 17000$ based on calibration with polystyrene (Fig. 3). Block copolymer formation is corroborated by the ^{1}H NMR spectrum, as the polymer obtained after the chain extension shows signals that are character-

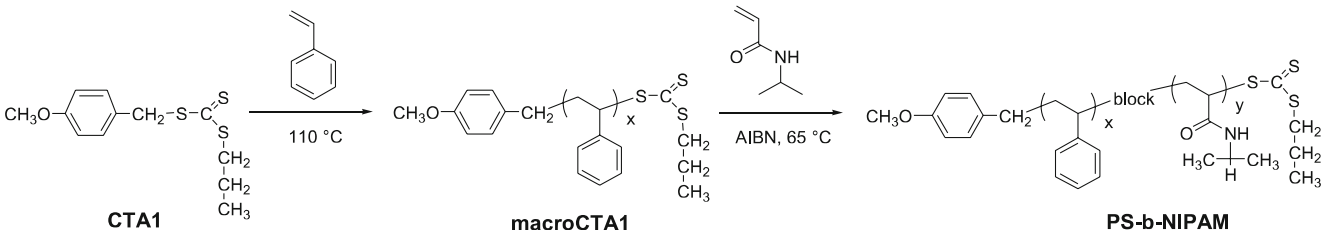

Scheme 1 Synthesis of diblock copolymer P(S-*b*-NIPAM) via successive RAFT polymerizations of styrene, using CTA1, and NIPAM

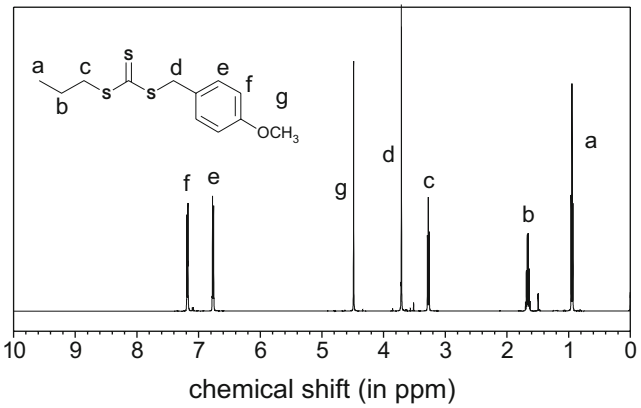

Fig. 1 The ^{1}H NMR spectrum of RAFT agent CTA1 in $CDCl_3$

istic of both homopolymers (Fig. 3). Concerning the true molar mass of the block copolymer, the spectrum also still allows to identify qualitatively some small signals that may be attributed to fragments of the R and Z groups as discussed above.

However, these signals are no more sufficiently resolved and seem also no more intense enough to allow meaningful integration for end-group analysis. Still, from the integrals of the signal groups at 4 ppm (characteristic for the CON–CH< proton of the NIPAM repeat unit) and at 6.4 to 7.6 ppm (characteristic for the CONH-proton of the NIPAM repeat unit and for the aromatic protons of the styrene repeat unit), one may estimate the molar mass of the block copolymers obtained, assuming that (1) the molar mass of the polystyrene block is preserved in the block copolymer and that (2) H–D exchange of the slightly acidic amide CONH proton is negligible. Therefore, integration was done for the spectra recorded in DMSO-d_6 instead of acetone. In this way, the molar mass M_n of the block copolymer is obtained as 22,600, i.e., the masses for the polystyrene and the PNIPAM blocks are 5,000 and 17,600, respectively.

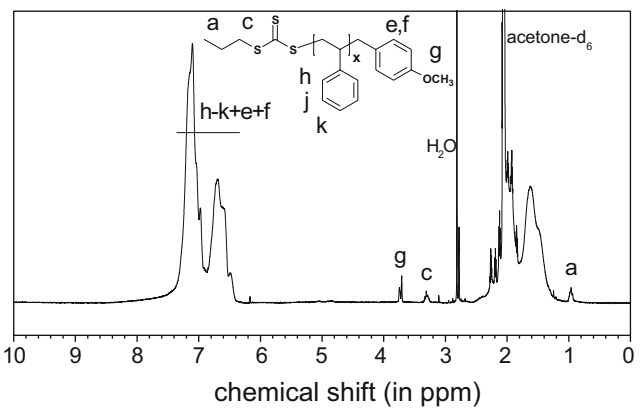

Fig. 2 The 300-MHz ^{1}H NMR spectrum of macroRAFT1 (polystyrene) in acetone-d_6

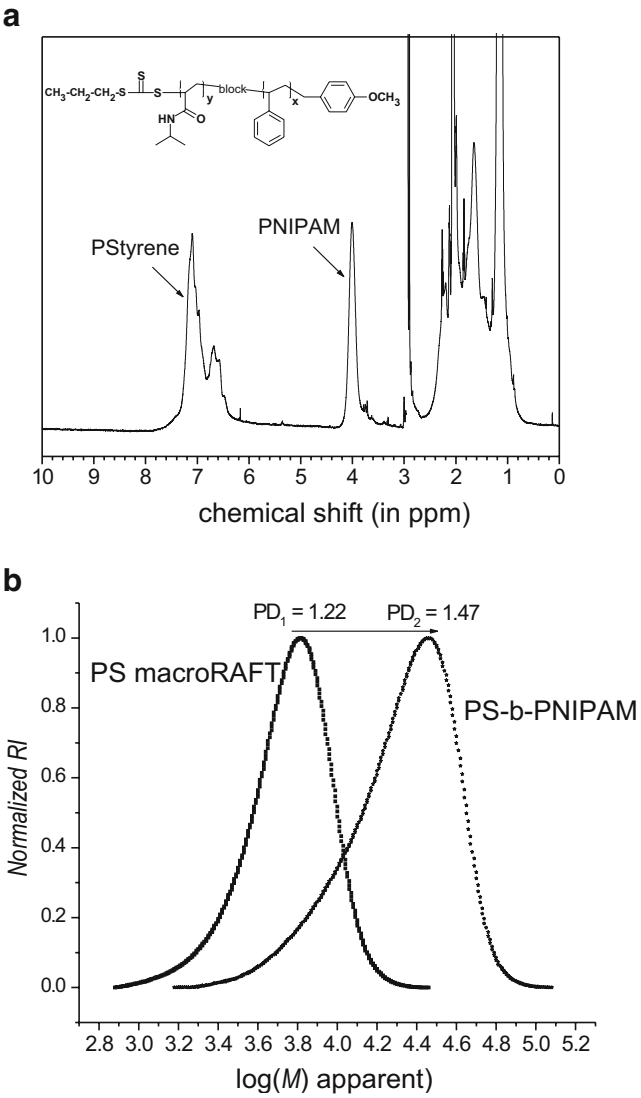

Fig. 3 Characterization of P(S-*b*-NIPAM): **a** ^{1}H NMR spectrum in acetone-d_6; **b** SEC elugrams of P(S-*b*-NIPAM) and its precursor PS macroRAFT1

The molar mass value of the block copolymer can be checked by elemental analysis, as the latter data enable to calculate the absolute molar mass, too, when assuming again that the molar mass of the polystyrene block is preserved in the block copolymer. Using the C/N ratio, which circumvents the problem due to the hygroscopy of the polymer, we determine the molar mass M_n of the block copolymer as 23,200; i.e., the masses for the polystyrene and the PNIPAM blocks are 5,000 and 18,200, respectively. The so found value may be less accurate than the one determined by ^{1}H-NMR, but the good agreement between the two methods is excellent. We conclude that the diblock copolymer has block molar masses of 5,000 g/mol for PS and 18,000 g/mol for PNIPAM, with an accuracy not better than 10%.

CMC of P(S-*b*-NIPAM) in aqueous solution

Different from most aggregation studies of block copolymers bearing PS as the hydrophobic block in water [31, 32], the copolymer is directly soluble in water due to the relatively short PS block. This facilitates a thorough study of its self-assembly in aqueous solution, starting from the CMC, the collapse at the LCST, and the micellar size and aggregation.

The CMCs of amphiphilic block copolymers are usually very low [33–37]. By means of FCS, the diffusion coefficients of fluorescent molecules can be determined at concentrations as low as in the nanomolar range. Using poorly water-soluble fluorescent dyes as tracers in aqueous P(S-*b*-NIPAM) solutions above the CMC, they attach to the micelles and can thus indicate their presence [38]. Below the CMC, the fluorescent molecules stay dissolved. We have used Rh6G as a tracer at low concentration (50 nM). Aqueous solutions of P(S-*b*-NIPAM) were prepared in a wide concentration range (~0.002–0.2 mg/ml). The resulting hydrodynamic radii are shown in Fig. 4a. At low concentrations, the correlation curves can be fitted with a single decay leading to R_h=1.0 nm, the value expected for Rh6G [38]. Above a polymer concentration of 0.028 mg/ml, a second, slower decay is present in the correlation curve (not shown) with hydrodynamic radii of 40 nm. The CMC has thus been reached, and a fraction of the Rh6G molecules are solubilized within the micelles. The fraction of Rh6G attached to micelles starts to increase at the same concentration (Fig. 4b); i.e., more and more dye molecules are solubilized in the micellar cores. At concentrations of 0.15 and 0.20 mg/ml, the R_h values coincide with the micellar hydrodynamic radius determined by DLS (see below). We conclude that the CMC of P(S-*b*-NIPAM) is located at 0.028 mg/ml (1.2 μM) and that micelles of an average hydrodynamic radius of 40 nm are formed.

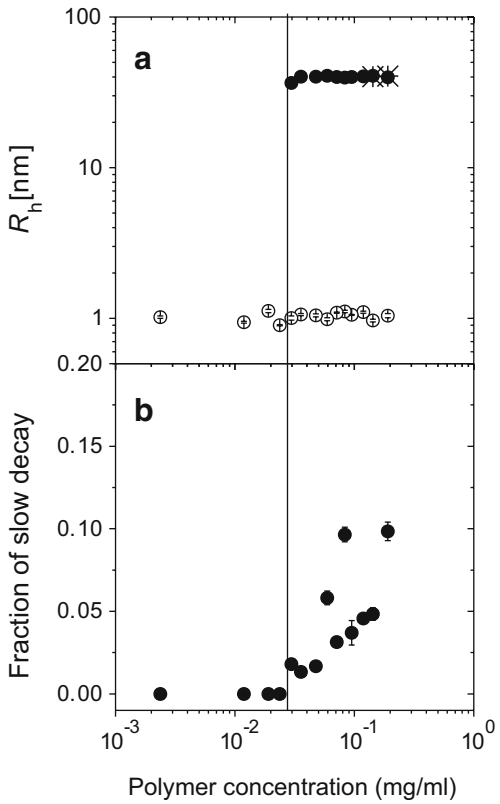

Fig. 4 Results from FCS on aqueous solutions of P(S-*b*-NIPAM) with Rh6G as tracers as a function of the copolymer concentration. The concentration of Rh6G was kept at 50 nM. The temperature was 27 °C. **a** Hydrodynamic radii of Rh6G (*unfilled circle*) and of the micelles (*filled circle*), both from FCS. *Asterisk* Micellar hydrodynamic radii from DLS. **b** Fraction of Rh6G bound to micelles

Collapse transition of PNIPAM

Microcalorimetry allowed us to determine the LCST temperatures of the PNIPAM block in the micellar solutions. Aqueous solutions having a concentration of 1.0 mg/ml were studied, thus a factor of ~40 above the CMC as determined by FCS. To rule out the effects due to the scan rate, rates between 0.5 and 1.0 K/min were applied. The resulting heat capacities show a single peak (Fig. 5). Its maximum position depends only weakly on scan rate and varies between 31.4 °C at 0.5 K/min and 31.9 °C at 1 K/min; i.e., the scan rates chosen are sufficiently low. In either case, we attribute the peak to the LCST of the PNIPAM blocks forming the shell of the micelles present in solution. The temperature range of the peak is broad (~20–45 °C). Both the peak temperature, the width of the peak and the shape are very similar to the results reported on an aqueous P(S-*b*-NIPAM) diblock copolymer solution with PS and PNIPAM block molar masses of 8,000 and 13,600 g/mol,

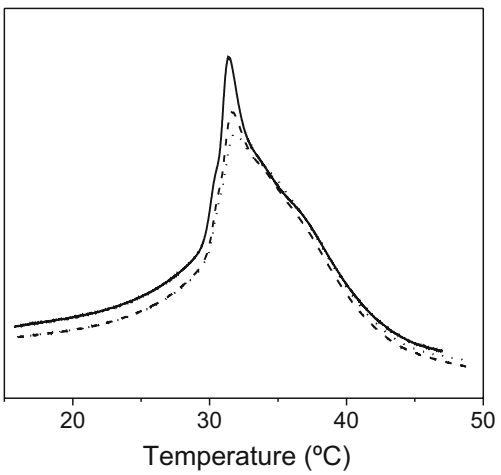

Fig. 5 Thermogram of a 1.0 mg/ml aqueous solution of the P(S-*b*-NIPAM) diblock copolymer at a heating rate of 0.5 K/min (*full line*), 0.75 K/min (*dashed line*), and 1.0 K/min (*dotted line*)

which was reported to form crew-cut micelles in aqueous solution [16]. The detailed origin of the shoulder on the high-temperature side of the main peak is unclear. It has not been observed in a P(S-*b*-NIPAM) diblock copolymer solution with PS and PNIPAM block molar masses of 5,000 and 39,100 g/mol, which was reported not to form micelles in aqueous solution [16]. We have not observed a shoulder in a hydrophobically end-capped PNIPAM homopolymer either [39]. We speculate that the shoulder is due to the fact that, in our system, PNIPAM forms the shell of a micelle and that all PNIPAM blocks are tethered to the surface of the PS core. The crowding of the shell near the PS core hinders dehydration, and therefore, the thermogram is broadened.

Turbidity measurements were carried out to relate the maximum in the thermogram to the LCST (Fig. 6). To be in the micellar solution regime, a concentration well above the CMC was chosen (0.2 mg/ml). The transmission decreases steeply above a temperature of 30.2 °C. It shows a shoulder at ~40 °C and reaches a plateau at 95% of the initial value at 55 °C. Upon cooling, hysteresis is observed between 40 and 25 °C, and the full transmission is nearly recovered. The process is thus fully reversible with a hysteresis loop. The onset of the decrease is only slightly lower than for the homopolymer PNIPAM, as repeatedly has been found for block copolymers containing PNIPAM [17, 40]. The polymer does not precipitate at elevated temperature, a phenomenon that has been discussed recently [41].

Structure of the micelles

In dynamic light scattering experiments, the hydrodynamic radius of the micelles was determined as a function of temperature. The same concentration as in turbidimetry was chosen (0.20 mg/ml) to minimize the turbidity above the LCST but high enough to give correlation functions with good statistics. The intensity autocorrelation functions were analyzed using the REPES algorithm, a model-free approach leading to distribution functions of hydrodynamic radii [26, 27]. Representative curves are shown in Fig. 7a. Up to 46 °C, the distribution curves reveal a single peak when a probability to reject $p=0.5$ is chosen, i.e., the most probable solution (solid lines in Fig. 7a). Whereas the distribution is relatively broad up to 31 °C, it becomes significantly more narrow above, and the maximum is shifted to smaller R_h values (dashed lines in Fig. 7a). We note that, even though the peak is broad, there is no evidence for the presence of two peaks. However, above 36 °C, the distributions seemingly become broader again with the maximum staying at the same position but a shoulder appearing on the right side of the peak (dotted lines in Fig. 7a). At temperatures above 46 °C, the peak splits up into two peaks with the left one being narrow again (dash-dotted lines in Fig. 7a).

The corresponding average hydrodynamic radii, i.e., the centers of gravity of the peaks, are given in Fig. 7b. Between 20 and 29 °C, the hydrodynamic radius decreases slightly from 42 to 39 nm. We assign these particles to swollen and polydisperse micelles. Between 29 and 32 °C, the value drops to 31 nm and stays at this value up to 36 °C. We attribute this decrease of micellar size at 29.5 °C to the collapse of the PNIPAM shell of the micelles at the LCST. The decrease of R_h from 39 to 31 nm corresponds to the collapse of the hydrophilic shell of the single micelle. When heating to 40 °C and cooling down again, this transition is reversible and shows no hysteresis.

At temperatures above 36 °C, the average R_h value increases again. This seems to be due to the rise of a shoulder on the right side of the peak (Fig. 7a) and points to the presence of larger aggregates. We have therefore additionally evaluated the correlation curves once more using a lower probablility to reject, namely $p=0.001$. The resulting curves are less smooth than the ones at $p=0.05$. This alternative analysis reproduces the peak at $R_h=31$ nm, which we attribute to collapsed micelles, and an additional peak having $R_h=70$–90 nm. We note that the REPES analysis is model-free; i.e., there is no possibility to fix the position of peaks. It is thus remarkable that the peak obtained below 36 °C is recovered at the same position just by lowering the degree of smoothing. This means that the micellar size does not depend on whether the micelles are free or arranged in clusters. At 55 and 60 °C, the peak splitting is observed even with $p=0.5$. The larger aggregates present above the LCST are clusters of collapsed (and therefore water-insoluble) micelles. The solutions are optically clear in the entire temperature range, which is in agreement with the relatively small cluster size of 70–90 nm.

We conclude that, using DLS, we have detected the LCST of the micelles at 29.5 °C. The size decrease of the micelles due to the collapse of the PNIPAM shell amounts to 26%. We note that using DLS, unimers are usually not detectable in the presence of micelles (e.g., [36]). The LCST temperature determined by DLS is slightly lower than the ones found with microcalorimetry (31.4 °C) and in turbidimetry (31.6 °C). We attribute this discrepancy to the difference of detection: In DLS, the collapse transition of the micelle was found from the point of inflection of the curve, where approximately half the micelles have collapsed. In microcalorimetry, in contrast, the peak is located at the temperature where most micelles have collapsed and is thus shifted into the direction of temperature change.

Comparing the results from turbidimetry and DLS may give a hint to the origin of the hysteresis observed in the turbidity (Fig. 6). DLS measurements were carried out at

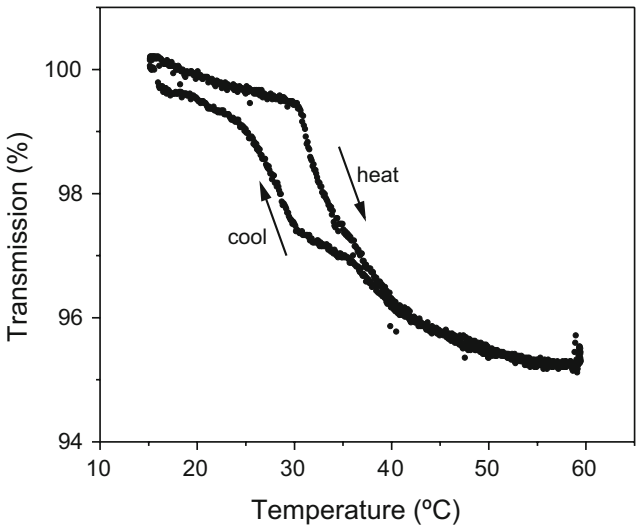

Fig. 6 Turbidimetry. Temperature-dependent transmission of a 0.2 mg/ml aqueous solution of P(S-*b*-NIPAM)

very low effective heating/cooling rates: For each temperature, the waiting time was 20 min and the measurement time 10 min. In turbidimetry, a much higher heating/cooling rate was applied (1 K/min), and the solution was heated to 60 °C. At this temperature, DLS revealed clusters. Upon cooling down from this temperature, a hysteresis loop was observed in turbidimetry. DLS showed that when cooling down from 40 °C, no hysteresis was observed (Fig. 7b). We conclude that the hysteresis upon cooling is due to the hindrance of swelling of the micellar shells when the micelles have formed clusters.

To determine the size of the micelles and to further characterize the collapse and the aggregates formed by the collapsed micelles, we carried out temperature-dependent SAXS experiments. Due to the low contrast (5% difference between the electron densities of PS and PNIPAM), the scattering is very weak. Even at the high-flux beamline A2 with counting times of 10 min, the statistics are only moderate. The SAXS curves from a solution having a concentration of 30 mg/ml show a decay, a minimum at $q \cong 0.30\ \mathrm{nm}^{-1}$ and another shallow maximum (Fig. 8). This shape is indicative of a micellar form factor from polydisperse micelles. A Guinier analysis [28] of the low q range results in a radius of gyration $R_g = 14.3$ nm at 20 °C. However, the fact that the electron densities of water and PS are nearly equal suggests a hollow sphere model. We have therefore fitted the form factor of a hollow sphere with a shell with an algebraic density decay to the curve at 20 °C (Fig. 8). A core radius of 11.1 nm with a relative standard deviation of 0.14 and an outer radius of 15.9 nm were obtained. The exponent of the density decay of the shell was found to be $\alpha = -0.5$. The shell thickness is thus 4.8 nm.

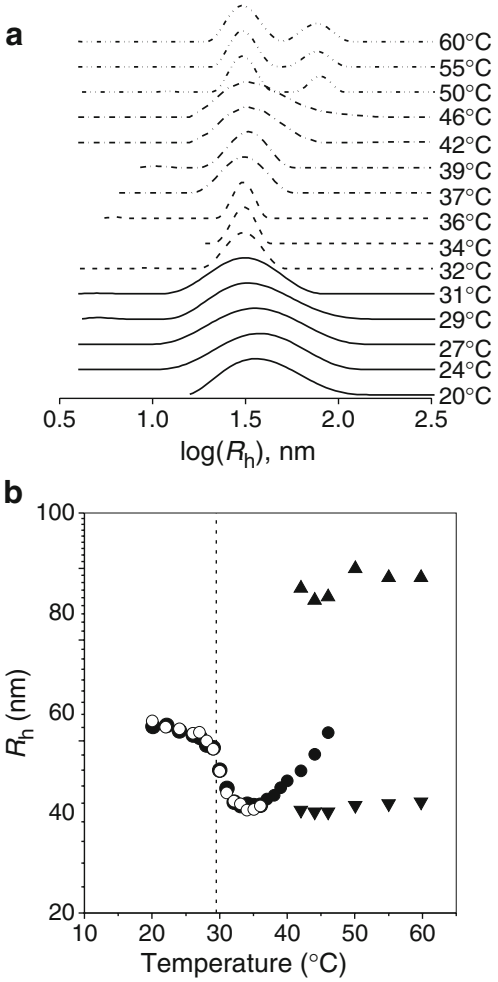

Fig. 7 Results from DLS at 0.20 mg/ml. **a** Representative distribution functions of hydrodynamic radii for different temperatures in equal area distribution R_h $A(R_h)$ vs. $\log(R_h)$. Heating run. The temperatures are given in the figure. The different line types represent the different regimes discussed in the text. The curves are shifted. **b** Resulting hydrodynamic radii of gyration as a function of temperature. *Filled circle* first heat, single decay with $p=0.5$; *open circle* second cool, single decay with $p=0.5$; **b**, *triangle* first heat, two peaks with $p=0.001$ or 0.5; see text. The *vertical line* denotes the point of inflection of R_h

At temperatures above 30 °C, a correlation peak is observed at $q_{max} = 0.31\ \mathrm{nm}^{-1}$. We attribute this peak to the average distance between the collapsed micelles in the cluster. This distance amounts to $2\pi/q_{max} \cong 20.3$ nm. Assuming tightly packed and compact micelles, their radius can be estimated to half their distance, i.e., 10.1 nm. To obtain more reliable values for the micellar size and distance, we have fitted a model where the interaction between micelles was taken into account using the Percus–Yevick structure factor (Fig. 8). As the statistics are not sufficiently good to obtain information on the core-shell structure, a model of a homogeneous sphere was used, comprising both the core and the collapsed shell. In this way, a sphere radius of 8.1 nm with a relative standard deviation of 0.15 was found. The hard-sphere radius from

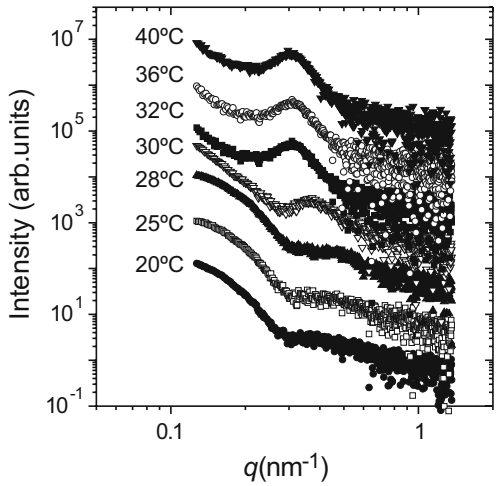

Fig. 8 SAXS curves of an aqueous polymer solution having a concentration of 30 mg/ml. Heating run. For clarity, the curves were shifted vertically by a factor of 8

the structure factor was 10.2 nm; the average distance between the centers of the micelles is thus 20.4 nm, in agreement with the position of the maximum discussed above. This radius is larger than the sphere radius; the micelles are thus not squeezed.

The decrease of the radius R between 20 and 40 °C is 45%, thus higher than the value from DLS. The difference may be due to different radii being monitored (the hydrodynamic radius R_h and the geometrical radius R). From SAXS measurements, we thus conclude that the collapse of the micelles is located at 30 °C, in agreement with microcalorimetry, turbidimetry, and DLS. The collapse of the micelles as well as their aggregation above the LCST temperature observed in DLS could be confirmed.

TEM allowed us to get a visual impression of the micelles at room temperature. Spherical objects were observed, which we attribute to the micelles (Fig. 9). An average radius of 11.0±0.5 nm was determined. This value may either be the radius of the dry micelles having a completely collapsed shell or the radius of the PS core immersed into loosely packed PNIPAM blocks that are invisible. This is in agreement with other TEM studies of P(S-*b*-NIPAM) diblock copolymers. For instance, the micelles formed by P(S-*b*-NIPAM) diblock copolymers with block molar masses of 8,000 g/mol for PS and 13,600 g/mol for PNIPAM do not show inner contrast due to a core-shell structure in cryo-TEM [16]. Only in high-resolution TEM from a P(S-*b*-NIPAM) diblock copolymer with block molar masses of 21,600 and 40,400 g/mol (i.e., much longer block lengths than our polymer) can a faint shell be discerned from the core [18]. These authors report on another P(S-*b*-NIPAM) diblock copolymer with block molar masses of 21,600 and 19,900 g/mol forming vesicles. In high-resolution TEM, only the voids can be discerned from the otherwise homogeneous polymer maxtrix.

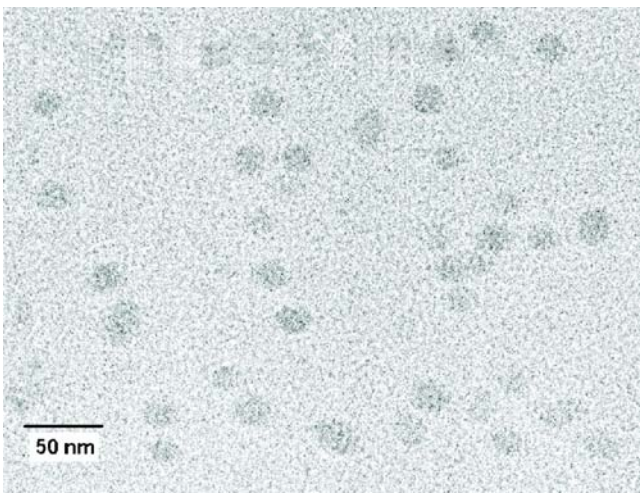

Fig. 9 Transmission electron micrograph prepared from a 0.10 mg/ml aqueous solution

For the solutions, we conclude that the LCST could be detected by means of various methods (Table 1), and the micellar size and correlation could be characterized. The polymer behaves similar to the diblock copolymer described by Nuopponen et al. [16] having block molar masses of 8,000 and 13,600 g/mol for PS and PNIPAM, respectively, even though the latter has a lower PNIPAM weight fraction than our copolymer: Both diblock copolymers form micelles in aqueous solution that show a collapse transition broader than the one of PNIPAM homopolymers. In both cases, the micelles are spherical and presumably of core-shell type. We have additionally detected the aggregation of micelles to clusters above the

Table 1 Results obtained from various methods

Method	T (°C)	R_h (nm)	R_g (nm)	R (nm)	LCST (°C)
FCS	RT	40	–	–	–
Microcalorimetry	–	–	–	–	31.4
Turbidimetry	–	–	–	–	31.6 (heat)
					29.5 (cool)
DLS	20	42	–	–	29.5 (heat)
	29	39	–	–	
	32–60	31	–	–	
SAXS	20	–	14.3	15.9	31 (heat)
	20			11.1[a]	
	40			8.1[b]	
				10.2[c]	
TEM	RT	–	–	11.0	–

R_h hydrodynamic radius of the micelles, R_g radius of gyration of the micelles, R radius of the micelles

[a] Core only

[b] Assuming a homogeneous sphere

[c] Hard-sphere radius

LCST temperature. The P(S-*b*-NIPAM**)** diblock copolymer described by Zhang et al. [18] having a PS molar mass of 21,600 g/mol and a PNIPAM molar mass of 40,400 g/mol has a much higher overall molar mass than our copolymer and a lower PNIPAM weight fraction (0.65). It forms micelles like our diblock copolymer; however, the decrease of R_g and R_h occurs over a broader temperature range (25–33 °C) than in our case (29–32 °C). The reason might be the stronger tethering of the PNIPAM to the PS core due to its lower weight fraction.

Another diblock copolymer, in contrast, behaves significantly differently [16]: The PS molar mass is 5,200 g/mol, i.e., very similar to our copolymer, but the PNIPAM molar mass is 39,100 g/mol, i.e., more than twice as high as in our copolymer. This polymer was reported to form large aggregates even at room temperature [16]. The structure of these aggregates was not investigated further; however, the authors speculated that no core-shell micelles were formed. This behavior was attributed to the high molar mass and the resulting space demand of the PNIPAM block. Comparing the results to the polymer described here, we note the difference in preparation: Whereas our polymer was directly dissolved in water, Nuopponen et al. prepared the aqueous solutions by dialysis from *N*,*N*-dimethylacetamide [16]. In the dialysis, the PS blocks are separated from each other, and the assembly to micelles might be hindered, especially because they are short compared to the PNIPAM blocks. Assuming that, in spite of this difference in preparation, both systems are in thermodynamic equilibrium, the results indicate that, for a given core size, there seems to be a stability limit for spherical micelles that depends on the length of the PNIPAM corona blocks, i.e., on the shell thickness. The shell thickness has been predicted to scale like $N_{\mathrm{corona}}^{2(1-\nu)/5}$, where N_{corona} is the degree of polymerization of the block forming the corona and ν=0.588 for a good solvent, the case considered here [42]. For the two copolymers, we calculate a ratio of shell thicknesses of 1.6. For the copolymer from [16], this would result in a shell thickness of 7.7 nm, which is closer to the core radius of 11.1 nm than the 4.8 nm found for our copolymer. Presumably, the ratio between the shell thickness and the core radius, as well as the degree of stretching of the PNIPAM block become unfavorable for higher PNIPAM weight fractions, which destabilizes the spherical micelles. We have thus identified the limit of stability of spherical core-shell micelles at a PNIPAM weight fraction between 0.78 and 0.88.

We could furthermore detect the CMC of P(S-*b*-NIPAM) at 0.028 mg/ml and have determined the average size of the aggregates of collapsed micelles formed above the LCST.

Lateral structures in thick films

The lateral structures in thick films were studied using SAXS, both for a dry film and a film in liquid water. The film thickness (>100 μm) is much higher than the chain dimensions or the micellar size, and we thus do not expect confinement effects. Immersing the film in liquid water within the SAXS sample chamber is expected to lead to a certain degree of swelling but not to dissolution of the film. We have studied the thermal behavior both in the dry and in the swollen state.

For a dry film, a structural peak is observed at q_{max}= 0.25 nm^{-1} (Fig. 10a), which becomes weaker upon heating but does not change position. Using the relation $D=2\pi/q_{\mathrm{max}}$, a lateral distance of ~25 nm can be estimated, which is assigned to the average repeat distance of the building blocks (presumably spheres [16]). Upon cooling, the peak position stays constant. The intensity does not fully recover, and the peak stays broad, which may be attributed to slight

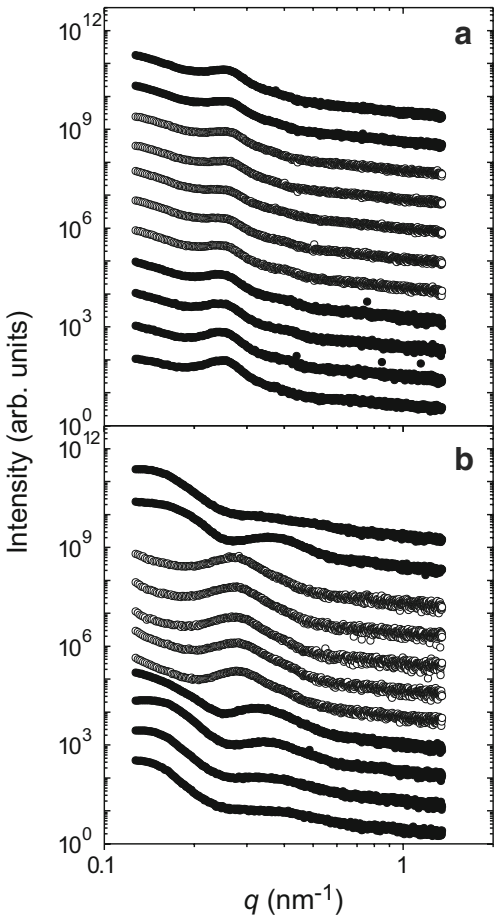

Fig. 10 Temperature-dependent SAXS intensity profiles of thick films. **a** Dry film and **b** film immersed in liquid water. The films were heated (starting from below) and subsequently cooled. The temperature sequence is 20, 25, 28, 30, 32, 36, 40, 36, 32, 28, 20 °C (from below). The curves were shifted vertically

changes in the arrangement of the spheres upon heating. No change is observed at the LCST observed in solution (30 °C), and we thus conclude that the collapse of the PNIPAM blocks does not occur in dry state as expected.

The situation is completely different when the thick film is immersed in water (Fig. 10b). At 20 °C, the curve resembles the form factor of a sphere: It shows a decay, a minimum at 0.25–0.26 nm^{-1}, and another broad fringe. Using the relation $R=4.5/q_{min}$ for the radius of a homogeneous sphere, we estimate a micellar radius R=17–18 nm. This value is similar to the one found in aqueous solution (15.9 nm), and we conclude that the micelles are swollen. Above 30 °C, the curves look completely different: A peak at ~0.28 nm^{-1} is observed, which stays constant in both position and intensity upon heating to 40 °C and cooling to 36 °C. Assigning the peak to the correlation between collapsed micelles, we estimate an average distance of 25 nm between them. Assuming that the collapsed micelles touch each other, their radius is ~13 nm, thus smaller than in the swollen state and similar to the one in aqueous solution (10.1 nm).

All changes in the thick hydrogel film are fully reversible upon cooling. Consequently, the structural changes in the films exposed to water are due to the collapse of micelles and their association above the LCST, as observed in solution. The LCST of the thick hydrogel films is located at 31 °C, thus at the same value as in aqueous solution.

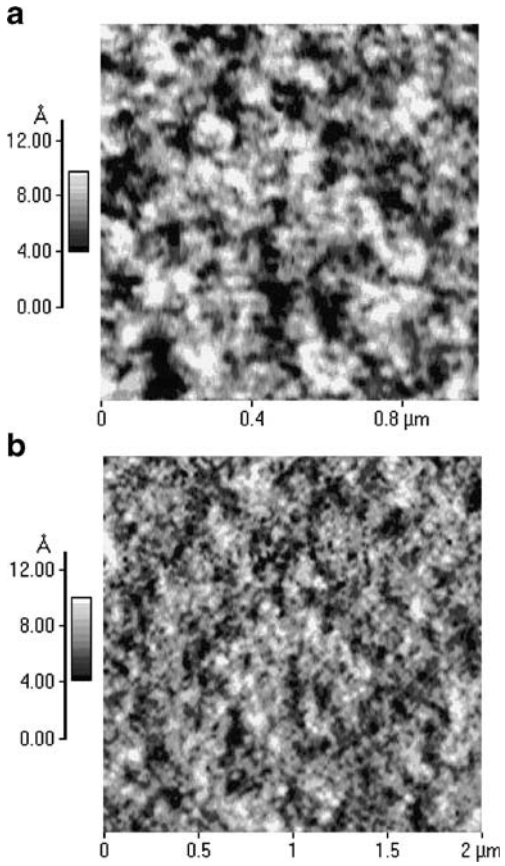

Fig. 11 AFM topography data of the dry film in a scan range of **a** 1×1 μm^2 and **b** 2×2 μm^2 to emphasize on the micellar structure and the larger surface structure formed by these micelles

Swelling behavior of thin films

To detect the influence of the confining thin film geometry and of the interaction with the substrate on the LCST behavior, we have investigated a thin film as well. The swelling behavior of a thin, spin-coated film was studied using optical interference measurements. The film thickness in dry state was 43.6 nm.

With AFM, the surface topography of the dry film was imaged (Fig. 11) using conditions as detailed in [39]. The film surface consists of spherical objects. Their mean particle diameter is 20 nm (Fig. 11a), and we identify them as micelles (Fig. 11a). The micelles are closely packed but do not fill space completely. Larger, non-periodic structures are created from the micellar building blocks (Fig. 11b). The phase images are featureless (not shown). However, due to the good agreement of the micellar size in solution and in the dry film, we conclude that the micellar core-shell structure is preserved in the thin film.

Exposed to saturated water vapor atmosphere, the film thickness increases to 76.3 nm (Fig. 12). The film thickness is now a factor of 5 higher than the micellar radius in aqueous solution. Upon heating in saturated water vapor, the film thickness stays constant up to 23 °C. It starts to decrease at 24 °C and reaches a value of 44 nm at 32 °C. This value persists up to 34 °C. The point of inflection is located at 26–27 °C. We conclude that the LCST of the P(S-*b*-PNIPAM) in thin-film geometry is depressed by several

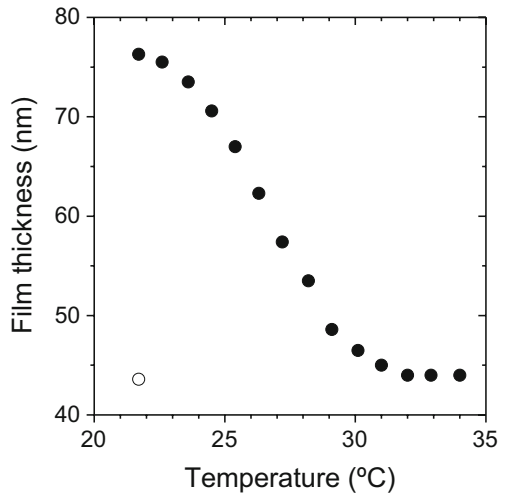

Fig. 12 Film thickness in the dry state (*open circle*) and during heating in saturated water vapor (*filled circle*)

degrees with respect to the solution and the thick film. A similar decrease in the LCST was observed in thin hydrogel films of end-capped PNIPAM [39]. This decrease was attributed to a subtle interplay between the interaction with the asymmetric walls (silicon substrate and vapor interface) and the possibility of water molecules to be released from a limited volume. Also in adsorbed cross-linked PNIPAM microgels, a small decrease of the LCST (1 °C) compared to the solution was observed [43].

The adsorption and structural transformation of micelles and vesicles formed by P(S-*b*- NIPAM) diblock copolymers on gold surfaces showed that the interaction between the polymer chains and the gold surface plays a critical role in the structural deformation and transformation. Micelles and vesicles without thiol groups underwent limited structural deformation and fusion when they were adsorbed on the surface. The micelles and vesicles with thiol groups were not only segmentally adsorbed but also tethered on the gold surface, leading to a large deformation and transformation [44].

Theoretically, a depletion of segments from the surface is present for a neutral or repulsive segment-surface interaction, and an excess of segments is present for an attractive interaction. The magnitude of the excess depends upon the strength of the attraction.

With neutron reflectivity, it was shown that a bilayer profile of end-tethered PNIPAM chains is present in D_2O. It indicates that the attraction of the NIPAM segments to the substrate surfaces is very strong, and a high-volume fraction of NIPAM segments in the surface layer forms [45]. Thus, we conclude that we have to expect intact P(S-*b*-NIPAM) micelles to build up in the thin film with PNIPAM segements preferentially enriched at the SiOx interface. This enrichment of PNIPAM segments at the substrate interface is independent of the total film thickness.

Summary

The structural changes upon a thermally induced transition from the swollen to a collapsed state between an aqueous solution, a thick and bulk-like film, and a thin film are compared for a P(S-*b*-NIPAM) diblock copolymer. Macroscopic properties and microscopic structures are correlated. Macroscopically, the diblock copolymer shows the expected behavior with the well-known LCST at 31 °C. In solution, micelles of core-shell type are present above the CMC. At the LCST, the hydrodynamic radius decreases by 26% due to the coil-to-globule collapse of PNIPAM in water, which is related to the release of water molecules from a polymer hydration layer into bulk water. The collapsed micelles form large aggregates.

We note that the block copolymer micelles presented in this paper are different from cross-linked core-shell latices in several aspects: When dissolving the copolymers in water, the micelles form by self-assembly, and the aggregation number is due to thermodynamic parameters. When preparing core-shell latices [12–15], the core size and shell thickness are determined by the monomer amounts used during synthesis. Moreover, in block copolymer micelles, each block is tethered to the surface of the (glassy) PS core. The density of the PNIPAM shell thus seems more inhomogeneous than the one of a cross-linked PNIPAM shell in the latices. The differences in the thermograms of the micelles and the latex solutions may be due to the stronger tethering of the PNIPAM blocks to the core and to their increased density near the PS core.

In the thick film, the behavior is identical, demonstrating that the gel character is based on physically cross-linked micelles, with the glassy PS blocks acting as links. Thus, for the investigated diblock copolymer, the behavior in the bulk, realized in the thick film, can be understood from the behavior in solution. In contrast, in a thin film, the transition shifts to lower temperatures due to the interaction with the substrate and the air interface. Moreover, the expansion is limited to a pure increase in thickness, which is a one-dimensional swelling, whereas the bulk samples and the micelles in solution can swell in all three directions in space. Due to the incompressibility of the solid substrate, the thin film can only expand by moving its interface with the water vapor atmosphere.

Acknowledgment We would like to thank R. Ivanova, M.-S. Appavou, and W. Doster, Physik Department E13, Technische Universität München; R. Luxenhofer, D. Weinfurtner and M. Hanzlik, Department Chemie, Technische Universität München, J. Rädler, Ludwig-Maximilians-Universität München; S. S. Funari, HASYLAB; and S. Förster, Universität Hamburg, for help with the measurements, data analysis, and fruitful discussions. We thank HASYLAB for providing us with a high-intensity X-ray beam and high-quality instrumentation. A.M.B.K. gratefully acknowledges a personal grant from Deutscher Akademischer Austauschdienst DAAD. Financial support by Deutsche Forschungsgemeinschaft within the priority program SPP 1259 (Pa771/4, Mu1487/8, La611/7) is gratefully acknowledged.

References

1. Schild HG (1992) Prog Polym Sci 17:163
2. Lin S-Y, Chen K-S, Chu L-R (1999) Polymer 40:2619
3. Percot A, Zhu XX, Lafleur M (2000) J Polym Sci Polym Phys 38:907
4. Katsumoto Y, Tanaka T, Sato H, Ozaki Y (2002) J Phys Chem A 106:3429
5. Hirokawa Y, Tanaka T, Matsuo ES (1984) J Chem Phys 81:6379
6. Housni A, Narain R (2007) Eur Poly J 43:4344
7. Shibayama M, Tanaka T, Han CC (1992) J Chem Phys 97:6829

8. Sato E, Tanaka T (1988) J Chem Phys 89:1695
9. Li Y, Tanaka T (1989) J Chem Phys 90:5161
10. Tanaka T, Sato E, Hirokawa Y, Hirotsu S, Peetermans J (1985) Phys Rev Lett 55:2455
11. Pelton RH, Chibante P (1986) Colloids Surf 20:247
12. Dingenouts N, Norhausen C, Ballauff M (1998) Macromolecules 31:8912
13. Kim J-H, Ballauff M (1999) Colloid Polym Sci 277:1210
14. Hellweg T, Dewhurst CD, Eimer W, Kratz K (2004) Langmuir 20:4330
15. Anderson M, Hietala S, Tenhu H, Maunu SL (2006) Colloid Polym Sci 284:1255
16. Nuopponen M, Ojala J, Tenhu H (2004) Polymer 45:3643
17. Mertoglu M, Garnier S, Laschewsky A, Skrabania K, Storsberg J (2005) Polymer 46:7726
18. Zhang W, Zhou X, Li H, Fang Y, Zhang G (2005) Macromolecules 38:909
19. Nykänen A, Nuopponen M, Laukkanen A, Hirvonen S-P, Rytelä M, Turunen O, Tenhu H, Mezzenga R, Ikkala O, Ruokolainen J (2007) Macromolecules 40:5827
20. Zhou X, Ye X, Zhang G (2007) J Phys Chem B 111:5111
21. Mayadunne RTA, Moad G, Rizzardo E (2002) Tetrah Lett. 43:6811
22. Postma A, Davis TP, Evans RA, Li G, Moad G, O'Shea MS (2006) Macromolecules 39:5293
23. Barner-Kowollik C, Buback M, Charleux B, Coote ML, Drache M, Fukuda T, Goto A, Klumperman B, Lowe AB, McLeary J, Moad G, Monteiro MJ, Sanderson RD, Tonge MP, Vana P (2006) J Polym Sci A Polym Chem 44:5809
24. Widengren J, Mets Ü, Rigler R (1995) J Phys Chem 99:13368
25. Magde D, Elson EL, Webb W (1974) Biopolymers 13:29
26. Jakeš J (1995) Coll Czech Chem Commun 60:1781
27. Štěpánek P (1993) In: Brown W (ed) Dynamic light scattering. The method and some applications. Clarendon, Oxford
28. Kratky O, Laggner P (1987) Encyclopedia of physical science and technology, vol 14, p 693
29. Förster S, Burger C (1998) Macromolecules 31:879
30. Müller-Buschbaum P (2003) Eur Phys J E 12:443
31. Riess G (2003) Prog Polym Sci 28:1107
32. Garnier S, Laschewsky A, Storsberg J (2006) Tenside Surfactants Deterg 43:88
33. Nivaggioli T, Alexandridis P, Hatton TA, Yekta A, Winnik MA (1994) Langmuir 11:730
34. Procházka K, Limpouchoá Z, Webber SE (1996) Block copolymer micelles. 2. Fluorimetric studies and computer modeling. In: Salamone JA (ed) Polymeric materials encyclopedia, vol 1 A–B. CRC, Boca Raton, pp 764–772
35. Schuch H, Klingler J, Rossmanith P, Frechen T, Gerst M, Feldthusen J, Müller AHE (2000) Macromolecules 33:1734
36. Bonné TB, Lüdtke K, Jordan R, Štěpánek P, Papadakis CM (2004) Coll Polym Sci 282:833
37. Bonné TB, Lüdtke K, Jordan R, Papadakis CM (2007) Macromol Chem Phys 208:1402
38. Bonné TB, Lüdtke K, Jordan R, Papadakis CM (2007) Coll Polym Sci 285:491
39. Wang W, Troll K, Kaune G, Metwalli E, Ruderer M, Skrabania K, Laschewsky A, Roth SV, Papadakis CM, Müller-Buschbaum P (2008) Macromolecules 41:3209
40. Arotçaréna M, Heise B, Ishaya S, Laschewsky A (2002) J Am Chem Soc 124:3787
41. Kujawa P, Aseyev V, Tenhu H, Winnik FM (2006) Macromolecules 39:7686
42. Zhulina EB, Birshtein TM (1985) Vysokomolekulyarnye Soedineniya 27:511 (English translation: (1986) Polym Sci USSR 27:570)
43. Schmidt S, Motschmann H, Hellweg T, von Klitzing R (2008) Polymer 49:749
44. Yan Y, Zhou X, Ji J, Yan L, Zhang G (2006) J Phys Chem B 110:21055
45. Yim H, Kent MS, Huber DL, Satija S, Majewski J, Smith GS (2003) Macromolecules 36:5244